

Enhanced elastic behavior of all-carbon composites reinforced by in-situ synthesized morphed graphene

H.A. Calderon^a, F. Alvarez Ramirez^{b,1}, D. Barber^{c,1}, V.G. Hadjiev^{d,**}, A. Okonkwo^{c,1}, R. Ordoñez Olivares^{e,1}, I. Estrada Guel^f, F.C. Robles Hernandez^{c,g,*}

^a Instituto Politécnico Nacional, Departamento de Física, ESFM-IPN, UPALM Ed. 9, Mexico CDMX 07738, Mexico

^b DITH, Instituto Mexicano del Petróleo, Eje Central Lázaro Cárdenas 152, 07730, Mexico City, Distrito Federal (DF), Mexico

^c College of Engineering Technology, University of Houston, Houston, TX, 77204-4020, USA

^d Texas Center for Superconductivity, Department of Mechanical Engineering, University of Houston, Houston, TX, 77204, USA

^e Mechanical and Materials Science and Engineering Department, University of Pittsburgh, 648 Benedum Hall, 3700 O'Hara Street, Pittsburgh, PA, 15261, USA

^f Centro de Investigación en Materiales Avanzados (CIMAV), Laboratorio Nacional de Nanotecnología, Miguel de Cervantes No. 120, C.P. 31136, Chihuahua, Chih, Mexico

^g Department of Materials Science and Engineering, and Computer Science and Electrical Engineering, University of Houston, Houston, TX, 77204, USA

ARTICLE INFO

Article history:

Received 13 May 2019

Received in revised form

18 June 2019

Accepted 3 July 2019

Available online 10 July 2019

ABSTRACT

We present the mechanical properties of all-carbon composites reinforced with in situ incorporated morphed graphene nanostructures by means of high energy ball milling and spark plasma sintering. The composites demonstrate enhanced elasticity for carbon sp^3/sp^2 ratio $\approx 1/4$. High resolution TEM characterization and molecular dynamics simulations show that this bonding type ratio is due mostly to the morphed graphene structures. Specifically, the presence of Rh6, crosslinked graphene-like, nanostructures is attributed to the enhanced elastic properties of these all-carbon composites. The improvements in mechanical properties is approximately 2 orders of magnitude when compared to similar composites produced with graphene.

Published by Elsevier Ltd.

1. Introduction

The development of all-carbon composites reinforced with carbon fibers has been investigated for several decades targeting key applications such as: thermal shock, wear, ablation, toughness and friction resistant [1]. The carbon fibers themselves have strengths of up to 4 GPa [2], that is, about four times stronger than modern steels [3]. The discovery of advanced carbon nanostructures has opened a new era in materials science, engineering and technology [4–7]. Pristine CNT have shown strengths [8] two orders of magnitude higher than that of advanced steels, titanium and super alloys [9]. Carbon reinforcements are desirable for their mechanical, electrical and thermal properties [10,11] and have been used in polymeric [12–14], textiles [15], metallic [16–19] and

ceramic [17,20–23] matrices. Well documented improvements for a variety of matrices include: hardness [17], toughness [20,24], electrical conductivity [22,24], and piezoelectric characteristics [25]. One of the most effective manufacturing practices involve mechanical milling and spark plasma sintering [22,26]. The improvement of properties of carbon reinforced materials, however, is typically below theoretical predictions by 2–3 orders of magnitude [18,27] mainly due to poor percolation, agglomeration and unwanted chemical reactions.

In the present work we provide evidence that the improved mechanical behavior observed in all-carbon composites is due to carbon allotropes called morphed graphenes. The composites were prepared from fullerene soot using mechanical milling and consolidated by means of spark plasma sintering. A unique characteristic of our composite processing technique is the in situ synthesis of morphed graphenes during milling. The results presented herein are supported by evidence gathered from various characterization methods, including X-ray diffraction (XRD), high resolution transmission electron microscopy (HRTEM), X-ray photoelectron spectroscopy (XPS), Raman spectroscopy, and numerical simulations based on molecular dynamics (MD).

* Corresponding author. College of Engineering Technology, University of Houston, Houston, TX, 77204-4020, USA.

** Corresponding author.

E-mail addresses: vhadjiev@uh.edu (V.G. Hadjiev), fcrobles@uh.edu (F.C. Robles Hernandez).

¹ Authors in alphabetic order and with equal contribution.

Mechanical properties were characterized by means of nanoindentation testing and successfully reproduced by MD simulations.

2. Experimental

The starting material was fullerene soot purchased from SERES Company. The milling was conducted on batches of 1 g in a high energy ball mill (SPEX) for 0, 0.5, 2, 5, 10, 20 and 50 h using steel hardened mills and milling media. The sintering was carried at 1500 °C in a spark plasma sintering system (SPS) at a heating rate of 140 °C/s for 1 min. The consolidated samples have dimensions of 12 mm in diameter and 4 mm in thickness. Sintering at lower temperatures was carried; however, the consolidation and densification were not as satisfactory. The sintered products were polished following standard metallographic procedures to a final finishing of 0.05- μm using a vibratory polisher for 3 h for metallography and nanoindentation.

X-ray diffraction (XRD) was carried in a D5000 SIEMENS diffractometer equipped with a Cu tube and a characteristic $K_{\alpha} = 0.15406 \text{ nm}$ operated a 40 kV and 30 mA. The SEM work was carried out on a FEI XL-30FEG operated at 15 kV. The transmission electron microscopy was conducted on the TEAM 0.5 microscope operated at 80 keV. Dose rate in use is below 10 cps equivalent to 12 $\text{e}^{-}/\text{\AA}^2\text{s}$ per image for a total dose of around 500 $\text{e}^{-}/\text{\AA}^2$. The Raman characterization was done on a confocal micro-Raman microscope XploRA™, Horiba JY. A 638 nm diode laser was used for excitation. The nanoindentation testing was carried in a Hysitron TI-900

TriboIndenter™ to obtain quantitative nanomechanical test results and real-time data collection. The loading environment is as follows: 7000 μN and 5 s dwelling time. The transducer used for this evaluation was a SN5-138-189 with a maximum Force: 9.562 mN. The hardness, stiffness and modulus were calculated following the standard procedures proposed in Ref. [28].

3. Experimental results and discussion

Fig. 1a presents the Raman spectrum of carbon soot used for synthesis of the all-carbon composites. It is worth noting that similar spectra are characteristic for a wide range of alternatives carbon with quasi-amorphous characteristics [29]. The spectrum features four main bands located at approximately 1320 cm^{-1} , 1580 cm^{-1} and 2665 cm^{-1} corresponding to the “D”, “G”, “2D” bands along with the combinational “D + G” two-phonon scattering [30] at 2900 cm^{-1} . It is expected that the main structure is a graphitic sp^2 type. The XRD results presented in Fig. 1 (b), however, show only one reflection at about $26.5^{\circ} - 2\theta$ degrees that is typical of the benzoic rings of graphitic structures. In graphite it corresponds to (002) XRD reflection. The absence of other reflections in the XRD spectra is a clear indication that there is no long range ordered graphite structure in this material. Instead, the order is short range, similar to that in amorphous carbon [27,31] and it is attributed to staking of sp^2 honeycomb lamellas. The HRTEM results in Fig. 1 (c) demonstrate that the raw material is amorphous with no evidence of graphitic domains. In conclusion, our

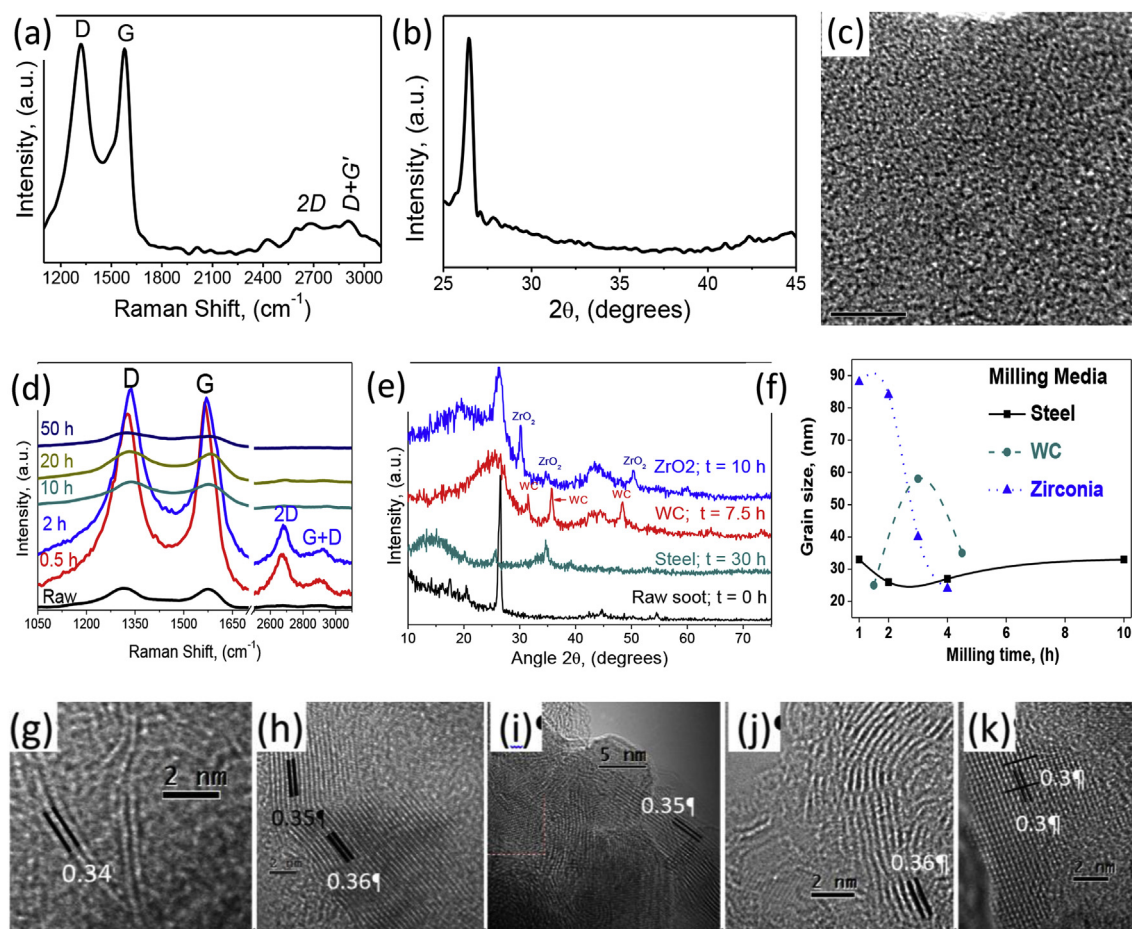


Fig. 1. Characterization of the fullerene soot milled for a series of periods of time: (a–c) raw and (d–f) milled samples. (a,d) characteristic Raman spectra, (b,e) XRD characterization. HRTEM for the samples milled in steel media (c) 0 h - raw soot, (g) 0.5 h, (h) 2 h, (i) 10 h, (j) 20 h, (k) 50 h. (A colour version of this figure can be viewed online.)

characterization confirms that the fullerene soot is mainly composed of short range order graphitic-like carbon.

The mechanically milled powders show a clear ordering in carbon nanostructures as a function of time. The prevalent mechanisms is associated with cold welding [32,33]. The Raman spectra in Fig. 1 (d) show the effects of milling on soot as a function of time and demonstrated that the largest amount in graphene (sp^2) bonding is observed at short milling times (<10 h). The intensity and width of the D band indicates that part of the carbon is amorphous and this is further confirmed with the HRTEM images in Fig. 1 (c) and 1(g–k). As far as contaminations are concerned, Fig. 1 (c) shows that hardened steel media introduce less impurities than zirconia and tungsten carbide media. The grain grow was calculated based on the Scherrer method and the results are presented in Fig. 1 (f).

Since the contamination of ceramic milling media (Fig. 1 (e)) was significantly above trace levels, we limited the research to steel media where the contamination was always way below 1 wt% Fe. The evolution of carbon nanostructures in material particles produced by varying milling time is depicted in Fig. 1(g–k). Previously, we have proposed the carbon structure called morphed graphene that has been characterized extensively [31] and modelled numerically. At short milling time one can observe double or triple layer graphenes followed by a multi-layer graphenes and then a

mix of multi-layer graphene and morphed graphenes. For longer milling time the dominating graphene-like phase is morphed graphene (e.g., Rh6 and Rh6-II) [31,34] though still embedded in amorphous carbon.

A higher abundance of Rh6 and Rh6-II in carbon nanostructured phases is observed in sintered samples of carbon milled longer than 10 h as demonstrated by HRTEM results shown in Fig. 2. A notable distinction between graphene and the morphed graphene is the d-spacing. The d-spacing in graphene is 0.33 nm [35], in morphed graphene varies from 0.35 to 0.37 nm for the Rh6 and Rh6-II structures, respectively [31,36]. Fig. 2 (a) shows a distribution of the phases identified in the microstructure. One of the very distinctive characteristics between the morphed graphene and graphene is an intermediate plane at approximately 0.175 nm in the former. HRTEM results in Fig. 2 reveal multiphase carbon composites that consist of graphene, Rh6, and Rh6-II embedded in amorphous carbon matrix. After the sintering, the carbon material reveal increased ordering or crystallinity of the phases and the amount of morphed graphene. To get further insight into the carbon structures we measured the sp^2 and sp^3 bonding balance using XPS. SEM images of the sintered composites are presented in Fig. S1 (e–f) in which large graphitic layers are seen as well as the layered structured of the consolidated product.

The XPS results shown in Table 1 reveal that the density of sp^3

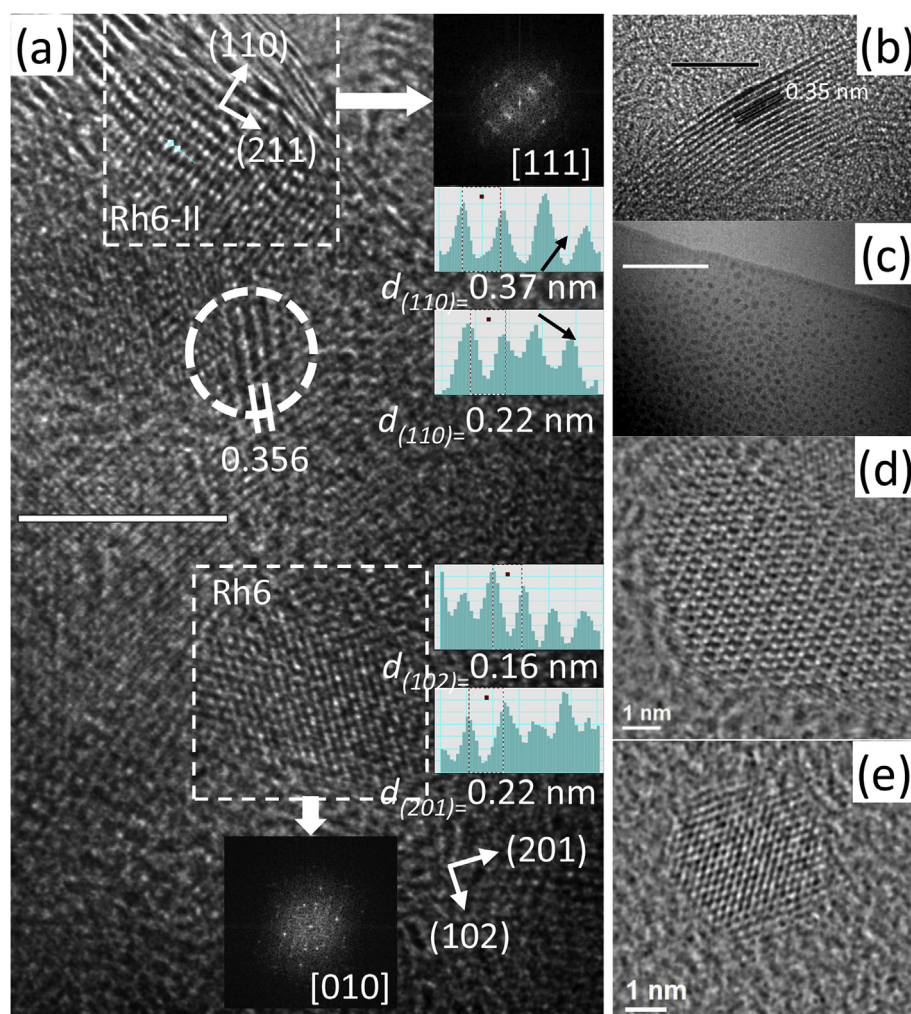


Fig. 2. Atomic resolution TEM analysis for various samples after sintering for 1 min at 1500 °C. Sample milled for (a) 10 h, (b) 2 h, (c–e) 20–50 h. (a) graphene (encircle) and morphed graphene (dashed squares) nanoparticles. (b–e) present a series of particles of morphed graphene with graphitic appearance to the more complex (Rh6-II) structure that is sp^3 in nature. (A colour version of this figure can be viewed online.)

Table 1
XPS results of the milled and SPS samples at 1500 °C for 1 min using a heating rate of 140 °C/s. The presence of iron (Fe) and the balance are the result of contamination due to the milling and sintering media. The oxygen present in the sample is identified forming various carbon species such as: C-O-H, C=O-H, CH_n, C=O. In the nanoindentation results the acronyms N, S, M stand for hardness, stiffness and modulus.

Mill. time (h)	Elements (at %)				Carbon Species (wt%)				Nanoindentation		
					Milled		SPS		H (GPa)	S (μN/nm)	M (GPa)
	C	O	Fe	Bal	sp ²	sp ³	sp ²	sp ³			
0	94	6	0	0	95.8	4.25	N/A	N/A	N/A	N/A	N/A
0.5	89.11	9.78	0.01	0.22	88	12	67	18	2.5 ± .5	34.7 ± 1	18.5 ± 2
2	85.65	12.64	1.03	0.78	87.1	12.9	63	16	2.2 ± .3	31.4 ± 1	15.6 ± 1
10	86.93	12.32	1.01	0.74	84.2	15.8	31	42	1.36 ± .3	30.5 ± 1	11.9 ± 1
20	93.46	5.99	0.55	0.0	81.8	18.2	77	19.8	0.82 ± .2	25.3 ± 2	7.6 ± 1
50	90.74	5.56	2.76	0.94	91.3	8.72	77.5	16.5	0.93 ± .2	31.1 ± 1	10 ± 0.5

bonding increases with milling time, reaching a maximum of 18.2% in the milled samples for 20 h, and it is attributed mostly to the Rh6-II phase. The SPS process further promotes the sp³ bonding, all sintered samples have more sp³ phases than in the milled ones. The increase of sp³ bonding reaches its maximum for the sintered sample milled for 10 h. With further increase of milling time the amount of sp³ phases in sintered samples drop in half. A possible mechanism for the Rh6-II phase amount increase is that it nucleates out of the regions having significant residual stresses or “bent” areas that give rise to the large abundance of round-like particles as presented in Fig. 2 (c).

The fact that the amount of sp³ fades at a longer milling time is due to excessive deformation or the breakage of the already existing crystals as it has been well documented [37]. Sintering is the key step that relieves by annealing the locations under high stresses and promotes the transformation to Rh6 type of structures [31,38]. The XPS results show that Fe contamination increases strongly after 20 h of milling and to investigate the actual benefits of morphed graphene one should focus to samples prepared for less than 20 h of milling. The raw sample did not consolidate during SPS because of it is fluffy (low density) and amorphous in nature.

Fig. 3 displays load – displacement (depth) curves for a nanoindentation test of selected samples milled at different time under load of 7000 μN that produces a contact depth (displacement) that ranges from 300 nm to 650 nm. In all cases the samples were SPS at 1500 °C for 1 min. Once the load is released, the corresponding plastic deformation under the indenter is basically nonexistent

(see, e.g., Fig. S2 (b)) but some residual displacement remains. This indicate a relaxation process typical for elastoplastic materials [28] with weak plastic deformation in contrast to that in martensite as shown in Fig. S2 (a). Table 1 presents the nanoindentation results. The higher hardness is achieved in composites milled for less than 10 h. The sample milled for 20 h possess the best elastic properties that is attributed to the presence of sp² carbon, mainly Rh6 structures, as demonstrated in Fig. 1(g–k) and Fig. 2. The elastic behavior deteriorates with increasing of sp³ bonding. Additionally, similar trends are observed for the stiffness and modulus. Therefore, the main elastic contributors herein are the morphed graphene type Rh6 having modulus of up to 1 TPa [39]. The outstanding recovery of the samples after nanoindentation tests results in permanent deformations 13.5%, 8.5% and 14.9% milled for 0.5, 2 and 20 h, respectively. The loading range in our nanoindentation test is two orders of magnitude higher than previously reported for composites manufactured under comparable conditions using pure graphene [28]. Here we can conclude that the presence of morphed graphene in all carbon composites have outstanding benefits.

The mechanical milling process is effective in two ways: at early stages it sponsors the synthesis of graphene and morphed graphene (Rh6) and as the milling time increases (above 10 h) the synthesis of Rh6 and Rh6-II prevails. In a similar work pure graphene platelets (no milling involved), sintered using SPS, show a plastic deformation of ~50% [40]. In this work the loading environment is 120 μN, that is, orders of magnitude lower than the load that applied (7 mN) in our tests and yet the composites behaving purely elastic. The mechanical testing results present a remarkable elastic behavior that has not been reported and is attributed to the in situ synthesis of morphed graphene, particularly the Rh6.

3.1. Molecular dynamics simulations of elastic properties

Although the elastic behavior of the material has been enlightened from an experimental mechanics viewpoint, its origin at the atomic level is not completely understood. In order to gain further insight into the enhanced elastic properties of the nanocomposites presented here, we performed molecular dynamics (MD) simulations on cell models with material bulk density in the range of our experimental results, that is, between 2.0 g/cm³ and 2.3 g/cm³. Initial structures are based on a graphite crystal cell with periodic conditions along the three axes. The cell dimension along x and y axes were fixing to 54.12 Å, whereas the length along the z axis change as function of bulk density. Subsequently, Rh6-II nanoparticles with diameters of 20 Å were incorporated to these cells and the entire model relaxed by a thermally annealing in molecular dynamics (MD) process using the GULP code [41] and the Tersoff force field [42,43]. From these three dimensional bulk models, we created a series of surface models with an empty space in the cells along [001] direction. A full outline of the construction of the

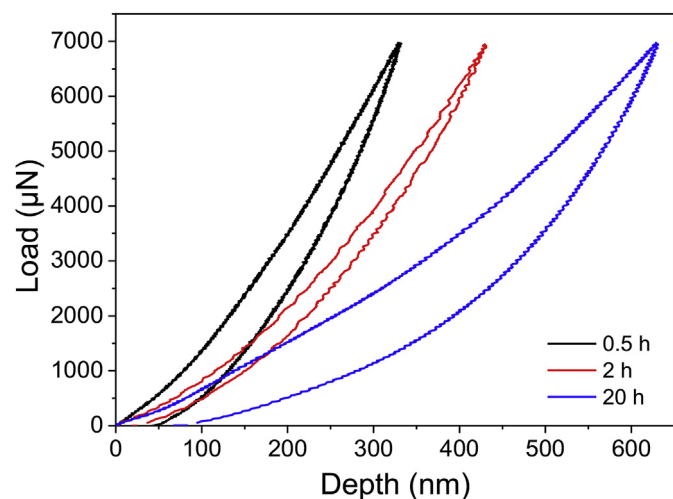


Fig. 3. Nanoindentation results for SPS consolidated samples milled at different times. The composition and mechanical properties of the samples are given in Table 1. (A colour version of this figure can be viewed online.)

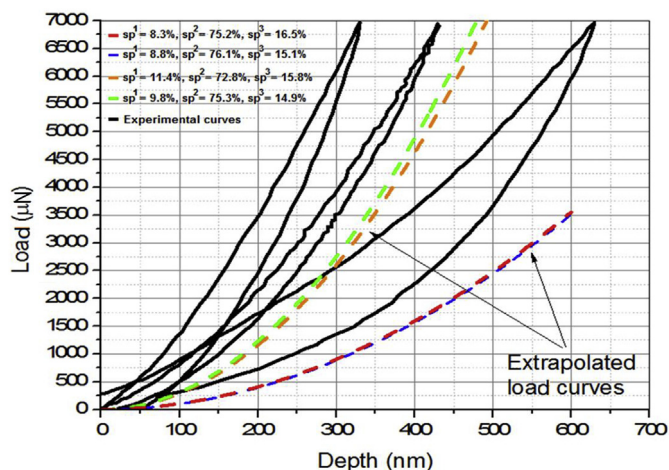


Fig. 4. Comparison between the experimental (shown in Fig. 3; highest to lowest slope: 0.5 h, 5 h, 20 h) and MD simulation load curves. The relative amount of different carbon hybridization for experimental samples is given in Table 1 and that of the simulated samples in the upper left corner of Fig. 4. The MD simulation curves were produced by extrapolation of the calculation results as described in the text. (A colour version of this figure can be viewed online.)

models and a more detailed description is presented in Fig. S3 of the Supplementary Information. From the set of bulk cells generated, we have selected 4 cells with sp^3/sp^2 hybridization ratio that is closest to experimental one reported in Table 1. The cutoff radius to determine the coordination of an atom was selected considering the first minimum of the function of radial distribution of the material, which in this case was 1.9 Å. This criterion is commonly used for the study of amorphous materials which meets the experimental and theoretical values in carbon-based materials. A detailed description of the distribution of the sp^1 , sp^2 and sp^3 fractions inside the simulation cells using this geometric criterion is given in Figs. S4–S7 of the Supplementary Material.

The elasticity of the models were determined by emulating the nanoindenter penetration process on the surface. We choose a rigid capped nanotube as a nanoindenter that was introduced in a succession of steps on the surface allowing a surface model relaxation

each time the nanoindenter penetration depth was increased. Relaxation of the system was obtained through a thermal MD annealing process at 1000 K during 1×10^4 simulation steps and using a time step of 1 fs. As a result of this succession of simulations, the energy of the system is mapped as a function of penetration depth. Because simulations at atomistic level that reach micras sizes are computationally nonviable, it is not possible to reach the experimental nanoindentation depths. To overcome this obstacle, we extrapolated the simulated behavior along the first nanometers of penetration to micrometric depths through polynomial fitting; for details see, e.g., Figs. S4–S7. Finally, the deformation force or the load was determined from the energy vs depth curves through the first derivative $F \propto dE/dx$, where dx is the penetration depth. The comparison between the extrapolated load vs depth curves obtained from simulation data and the experimental nanoindentation results is shown in Fig. 4.

The force field used in the MD simulation was limited in reproducing completely the Rh6 structure. The crosslinking observed in MD simulations between the graphite sheets, however, resemble those found in crystalline structures type Rh6. An example of this similarity is given in Fig. 5, in which the simulated spongy structure in Fig. 5(a and b) concurs with the crosslinked graphene-like layers of the Rh6 structure in Fig. 5(c and d). We believe that the crosslinking that is inherent for the Rh6 and Rh6-II structures plays an important role in enhancement of mechanical properties of all-carbon composites.

4. Conclusions

We have presented the mechanical properties of all carbon nanocomposites prepared with in situ incorporated morphed graphene structures. The presence of Rh6, sp^2 type, morphed graphene is attributed to the enhanced elastic properties of these all carbon nanocomposites over those prepared only from graphene. The MD modeling shows that the material densities that best reproduce the mechanical properties of the reported all-carbon composites are between 2.1 and 2.3 g/cm³. In this density range it is possible to generate bonds between the graphite sheets, crosslinks, which improve their elastic response with respect to the non-crosslinked graphite sheets. The similarity of the simulated crosslinking

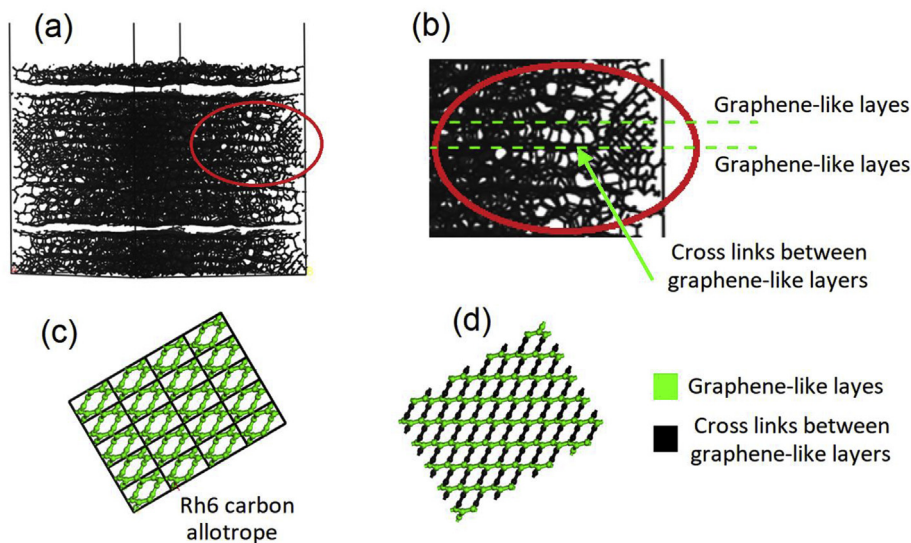


Fig. 5. (a) View of a simulation cell with carbon hybridization distribution: $sp^1 = 11.4\%$, $sp^2 = 72.8\%$, $sp^3 = 15.8\%$. More details of simulation cells are given in Figs. S4–S7. (b) Zoom region showing presence of crosslinks (highlighted) between graphene-like layers. (c–d) Two projections of the crystal structure of Rh6 carbon allotrope. Graphene-like and crosslinking regions are depicted by different colors. (A colour version of this figure can be viewed online.)

structure of graphene sheets with that of Rh6 and the experimental (HRTEM) observation of Rh6 in the all-carbon composites lend support to the claim that Rh6 morphed graphene is mostly responsible for the enhanced elastic properties of the composites.

Acknowledgments

The authors would like to express their gratitude to Dr. D. Butt (currently at University of Utah) for facilitating the Spark Plasma Sintering facilities at Center for the Advanced of Energy Studies (CAES) at Idaho Falls. VGH work was supported by the State of Texas through the Texas Center for Superconductivity (TcSUH) at the University of Houston. Work at the Molecular Foundry was supported by the Office of Science, Office of Basic Energy Sciences, of the U.S. Department of Energy under Contract No. DE-AC02-05CH11231.

Appendix A. Supplementary data

Supplementary data to this article can be found online at <https://doi.org/10.1016/j.carbon.2019.07.012>.

References

- [1] J.E. Sheehan, K.W. Buesking, B.J. Sullivan, Carbon-carbon composites, *Annu. Rev. Mater. Sci.* 24 (1994) 19–44.
- [2] F. von Sturm, Graphite fibers and filaments, in: M.S. Dresselhaus, G. Dresselhaus, K. Sugihara, I.L. Spain, H.A. Goldberg (Eds.), *Springer Series in Materials Science*, vol. 5, Springer, Berlin/Heidelberg, 1988, x, 382 pp., hard cover, DM 122.00.—ISBN 3-540-18938-6, *Adv Mater* 1(4) (1989) 130–131.
- [3] R. Ordóñez Olivares, C.I. Garcia, A. DeArdo, S. Kalay, F.C. Robles Hernández, Advanced metallurgical alloy design and thermomechanical processing for rails steels for North American heavy haul use, *Wear* 271 (1–2) (2011) 364–373.
- [4] H.W. Kroto, J.R. Heath, S.C. O'Brien, R.F. Curl, R.E. Smalley, C-60 - buckminsterfullerene, *Nature* 318 (6042) (1985) 162–163.
- [5] S. Iijima, Helical microtubules of graphitic carbon, *Nature* 354 (6348) (1991) 56–58.
- [6] K.S. Novoselov, A.K. Geim, S.V. Morozov, D. Jiang, Y. Zhang, S.V. Dubonos, I.V. Grigorieva, A.A. Firsov, Electric field effect in atomically thin carbon films, *Science* 306 (5296) (2004) 666–669.
- [7] J.-T. Wang, Y. Qian, H. Weng, E. Wang, C. Chen, Three-dimensional crystalline modification of graphene in all-sp² hexagonal lattices with or without topological nodal lines, *J. Phys. Chem. Lett.* 10 (10) (2019) 2515–2521.
- [8] C. Lee, X.D. Wei, J.W. Kysar, J. Hone, Measurement of the elastic properties and intrinsic strength of monolayer graphene, *Science* 321 (5887) (2008) 385–388.
- [9] J.R. Davis, A.I.H. Committee, *Metals Handbook*, Asm International, 1998.
- [10] S. Stankovich, D.A. Dikin, G.H.B. Dommett, K.M. Kohlhaas, E.J. Zimney, E.A. Stach, R.D. Piner, S.T. Nguyen, R.S. Ruoff, Graphene-based composite materials, *Nature* 442 (7100) (2006) 282–286.
- [11] S.H. Xie, Y.Y. Liu, J.Y. Li, Comparison of the effective conductivity between composites reinforced by graphene nanosheets and carbon nanotubes, *Appl. Phys. Lett.* 92 (24) (2008).
- [12] S.R. Bakshi, D. Lahiri, A. Agarwal, Carbon nanotube reinforced metal matrix composites - a review, *Int. Mater. Rev.* 55 (1) (2010) 41–64.
- [13] J.N. Coleman, U. Khan, W.J. Blau, Y.K. Gun'ko, Small but strong: a review of the mechanical properties of carbon nanotube-polymer composites, *Carbon* 44 (9) (2006) 1624–1652.
- [14] S.J.V. Frankland, A. Caglar, D.W. Brenner, M. Griebel, Molecular simulation of the influence of chemical cross-links on the shear strength of carbon nanotube-polymer interfaces, *J. Phys. Chem. B* 106 (12) (2002) 3046–3048.
- [15] A.B. Dalton, S. Collins, E. Munoz, J.M. Razal, V.H. Ebron, J.P. Ferraris, J.N. Coleman, B.G. Kim, R.H. Baughman, Super-tough carbon-nanotube fibres - these extraordinary composite fibres can be woven into electronic textiles, *Nature* 423 (6941) (2003) 703, 703.
- [16] F.C. Robles-Hernández, Production and Characterization of (Al, Fe)-C (Graphite or Fullerene) Composites Prepared by Mechanical Alloying, Metallurgy, Materials Science and Engineering, Instituto Politécnico Nacional, Mexico City Mexico, 1999, p. 150.
- [17] V. Garibay-Feblés, H.A. Calderon, F.C. Robles-Hernandez, M. Umemoto, K. Masuyama, J.G. Cabanas-Moreno, Production and characterization of (Al, Fe)-C (graphite or fullerene) composites prepared by mechanical alloying, *Mater. Manuf. Process.* 15 (4) (2000) 547–567.
- [18] F.C. Robles-Hernandez, H.A. Calderon, Nanostructured metal composites reinforced with fullerenes, *Jom-Us* 62 (2) (2010) 63–68.
- [19] R. Perez-Bustamante, I. Estrada-Guel, P. Amezaga-Madrid, M. Miki-Yoshida, J.M. Herrera-Ramirez, R. Martinez-Sanchez, Microstructural characterization of Al-MWCNT composites produced by mechanical milling and hot extrusion, *J. Alloy. Comp.* 495 (2) (2010) 399–402.
- [20] G.D. Zhan, J. Kuntz, J. Wan, J. Garay, A.K. Mukherjee, Alumina-based nanocomposites consolidated by spark plasma sintering, *Scr. Mater.* 47 (11) (2002) 737–741.
- [21] G.D. Zhan, J. Kuntz, J. Wan, J. Garay, A.K. Mukherjee, A novel processing route to develop a dense nanocrystalline alumina matrix (< 100 nm) nanocomposite material, *J. Am. Ceram. Soc.* 86 (1) (2003) 200–202.
- [22] G.D. Zhan, J.D. Kuntz, J.E. Garay, A.K. Mukherjee, Electrical properties of nanoceramics reinforced with ropes of single-walled carbon nanotubes, *Appl. Phys. Lett.* 83 (6) (2003) 1228–1230.
- [23] L.S. Walker, V.R. Marotto, M.A. Rafiee, N. Koratkar, E.L. Corral, Toughening in graphene ceramic composites, *ACS Nano* 5 (4) (2011) 3182–3190.
- [24] A.E. Fals, V.G. Hadjiev, F.C. Robles Hernández, Multi-functional fullerene soot/alumina composites with improved toughness and electrical conductivity, *Mater. Sci. Eng. A* 558 (0) (2012) 13–20.
- [25] B.C. Thompson, J.M.J. Frechet, Organic photovoltaics - polymer-fullerene composite solar cells, *Angew. Chem. Int. Ed.* 47 (1) (2008) 58–77.
- [26] U. Anselmi-Tamburini, J.E. Garay, Z.A. Munir, Fundamental investigations on the spark plasma sintering/synthesis process III. Current effect on reactivity, *Mat Sci Eng a-Struct* 407 (1–2) (2005) 24–30.
- [27] F.C. Robles Hernández, H.A. Calderon, Nanostructured Al/Al₄C₃ composites reinforced with graphite or fullerene and manufactured by mechanical milling and spark plasma sintering, *Mater. Chem. Phys.* 132 (2) (2012) 815–822.
- [28] W.C. Oliver, G.M. Pharr, An improved technique for determining hardness and elastic modulus using load and displacement sensing indentation experiments, *J. Mater. Res.* 7 (6) (2011) 1564–1583.
- [29] I. Estrada-Guel, O. Anderson-Okonkwo, F.C. Robles-Hernandez, In-situ transformation of amorphous soot into carbon-nanostructures by high-energy ball milling, *Microsc. Microanal.* 22 (S3) (2016) 1902–1903.
- [30] Z.H. Dong, P. Zhou, J.M. Holden, P.C. Eklund, M.S. Dresselhaus, G. Dresselhaus, Observation of higher-order Raman modes in C-60 films, *Phys. Rev. B* 48 (4) (1993) 2862–2865.
- [31] H.A. Calderon, I. Estrada-Guel, F. Alvarez-Ramírez, V.G. Hadjiev, F.C. Robles Hernandez, Morphed graphene nanostructures: experimental evidence for existence, *Carbon* 102 (2016) 288–296.
- [32] J.S. Benjamin, Fundamentals of mechanical alloying, *Mech. Alloy.* 88 (1992) 1–17.
- [33] C. Suryanarayana, Mechanical alloying and milling, *Prog. Mater. Sci.* 46 (1–2) (2001) 1–184.
- [34] J.-T. Wang, H. Weng, S. Nie, Z. Fang, Y. Kawazoe, C. Chen, Body-centered orthorhombic C_{16} : a novel topological node-line semimetal, *Phys. Rev. Lett.* 116 (19) (2016) 195501.
- [35] K.K. Sadasivuni, D. Ponnamma, S. Thomas, Y. Grohens, Evolution from graphite to graphene elastomer composites, *Prog. Polym. Sci.* 39 (4) (2014) 749–780.
- [36] H.A. Calderon, A. Okonkwo, I. Estrada-Guel, V.G. Hadjiev, F. Alvarez-Ramírez, F.C. Robles Hernandez, HRTEM low dose: the unfold of the morphed graphene, from amorphous carbon to morphed graphenes, *Adv Struct Chem Imaging* 2 (2017) 10.
- [37] J.S. Benjamin, Frontiers of high temperature materials, in: *Proceedings of an International Conference on Oxide Dispersion Strengthened Superalloys by Mechanical Alloying*, Held in New York City, May 18–21, 1981, IncoMAP, Suffern, N.Y., 1983.
- [38] F.C. Robles-Hernández, H.A. Calderon, Nanostructured metal composites reinforced with fullerenes, *JOM* 62 (2) (2010) 63–68.
- [39] I.W. Frank, D.M. Tanenbaum, A.M. Van der Zande, P.L. McEuen, Mechanical properties of suspended graphene sheets, *J. Vac. Sci. Technol. B* 25 (6) (2007) 2558–2561.
- [40] A. Nieto, D. Lahiri, A. Agarwal, Synthesis and properties of bulk graphene nanoplatelets consolidated by spark plasma sintering, *Carbon* 50 (11) (2012) 4068–4077.
- [41] J.D. Gale, A.L. Rohl, The general utility lattice program (GULP), *Mol. Simul.* 29 (5) (2003) 291–341.
- [42] J. Tersoff, New empirical approach for the structure and energy of covalent systems, *Phys. Rev. B* 37 (12) (1988) 6991–7000.
- [43] A.A. Valladares, J.A. Díaz-Celaya, J. Galván-Colín, L.M. Mejía-Mendoza, J.A. Reyes-Retana, R.M. Valladares, A. Valladares, F. Alvarez-Ramírez, D. Qu, J. Shen, New approaches to the computer simulation of amorphous alloys: a review, *Materials* 4 (4) (2011) 716–781.